Pergamon

0022-3697(95)00079-8

J. Phys. Chem. Solids Vol 56, No. 10, pp. 1425–1431, 1995

0022-3697/95 $9.50 + 0.00

TWO-BENT-CRYSTAL TECHNIQUE IN NEUTRON SMALL ANGLE SCATTERING

M. POPOVICI,† W. B. YELON,† R. BERLINER† and B. J. HEUSER‡

†Missouri University Research Reactor, Columbia, MO 65211, U.S.A.
‡University of Illinois, Nuclear Engineering Department, Urbana, IL 61801, U.S.A.

(*Received* 18 *January* 1995; *accepted* 20 *January* 1995)

Abstract—The design of two-bent-crystal small angle neutron scattering configurations is discussed. Neutron optics computations for experiment optimization are presented. An arrangement implemented at the Missouri University Research Reactor is described. It consists of a curved pyrolytic graphite pre-monochromator followed by two curved thin silicon wafers diffracting from (111) and (220) planes, respectively.

Keywords: C. neutron scattering.

1. INTRODUCTION

Small angle neutron scattering (SANS) can be measured with either pinhole instruments or two-crystal arrangements. In the latter method (which for X-rays is quite old [1] but for neutrons was only introduced in the 1970s [2, 3]) the sample is placed between two crystals and the rocking curve (intensity vs rotation angle of the second crystal) is measured. The difference between the intensities with and without sample is related to the small angle scattering (integrated over one dimension). Identical flat perfect crystals in non-dispersive parallel (+, −) setting are commonly used. Channel-cut perfect crystals with multiple reflections are used for X-rays to drastically reduce the wings of the rocking curve [4], allowing measurements at low background.

With neutrons, flat perfect crystals give very low intensities. Often the corresponding resolution is much too good and could well be sacrificed for intensity. This is not easily done, though. Mosaic crystals have wider reflectivity curves, but these have extended wings and thus the measurement range is limited by the high background [3]. Broader reflectivity curves can also be obtained by bending perfect crystals. However, the double reflection efficiency with identical crystals in parallel setting decreases on bending [5]. Such a decrease is known to occur in heat-loaded monochromators for synchrotron radiation (SR). As SR sources are sharp, the problem can be corrected by bending the second crystal to accommodate the curvature of the first [6]. With neutrons the problem is more severe, because sources are extended, and with identical crystals cannot be corrected.

The first experiments on bent two-crystal SANS have used identical crystals [7]. The double reflection efficiency was found to go down on bending, but the gain from the reflectivity broadening allowed an optimum to be reached. A way to get around the reflection efficiency problem was proposed [8] and implemented [9]: instead of measuring rocking curves, a position sensitive detector (PSD) was used. As the scattering by the sample also broadens the beam spatially, SANS can be measured at fixed orientation of the second crystal. The lower reflection efficiency is compensated by measuring with PSD many points at a time.

With bent crystals, an equivalent of the non-dispersive (+, −) setting of identical flat crystals exists [5]: it requires either an anti-parallel (+, +) setting of identical crystals or different d-spacings of the two crystals in any setting. We proposed [10] to use this as an alternative solution to the double reflection efficiency problem in SANS. The (331) and (400) reflections from thin silicon wafers were used to demonstrate the feasibility of the method at the Missouri University Research Reactor (MURR) [10].

We then considered the design of optimal two-bent-crystal SANS configurations, stimulated by plans at the Oak Ridge National Laboratory (ORNL) to implement such a configuration there. We found that a bent pre-monochromator may be quite useful. It not only reduces the background substantially, but facilitates spatial focusing: by placing the first crystal of the SANS pair in micro-focusing (+, +) setting to the pre-monochromator one can achieve flux gains [11]. These gains may more than compensate for the loss of intensity on reflection by the pre-monochromator. Focusing is

still possible with flat mosaic pre-monochromators [12].

The successive (111) and (220) reflections from standard thin silicon wafers appear to be the most interesting. SANS configurations with these reflections have been implemented: at MURR [13] with bent pyrolytic graphite (PG) pre-monochromator at 1.5 Å, and at ORNL with flat mosaic Si (111) pre-monochromator at 2.6 Å. Some experimental data obtained on the MURR configuration have already been reported [14, 15]. This paper presents the design principle of the method, neutron optics optimization computations and their experimental verification, and gives details on the experimental arrangement implemented at MURR.

2. THEORY

In the terminology used below, the 'pre-monochromator' is the crystal in the white beam, the 'monochromator' and the 'analyzer' are the first and the second crystals in the SANS pair (the second and third in sequence). The sample is thus placed between monochromator and analyzer. The configuration corresponds to three-axis spectrometers with the 'monochromator' at the usual sample position. We shall use the subscripts P, M and A for the quantities related to the pre-monochromator, monochromator and analyzer.

The efficiency of successive reflections is high if the phase space emergence and acceptance windows of the crystals involved match each other. Such a matching occurs naturally for identical flat crystals in parallel (+, −) setting. The decrease in the reflection efficiency of identical crystals is due to that matching being altered by a misfit between the corresponding phase space windows that develops on bending.

The matching conditions are obtained by considering the optics of successive Bragg reflections by bent crystals in the phase space [5]. In the diffraction plane, neutrons have three phase space coordinates $(\Delta k, \gamma, y)$: the deviation Δk from the average wavevector k, the deviation angle γ from the beam axis (actually it is $k\gamma$ which is truly a phase space coordinate) and the spatial coordinate across the beam y.

Let us first consider the reference case of flat perfect crystals. As the Bragg law is actually vectorial, its differential consists of three relations. The two relations referring to the diffraction plane are [16]:

$$(\Delta k/k)\tan\theta = \xi + \gamma_0 = b\xi - \gamma, \qquad (1)$$

where θ is the Bragg angle, γ_0 and γ are the angular deviations before and after reflection, ξ is the variable of the reflectivity (Darwin) curve, and b is the asymmetry parameter, $b = \sin(\theta + \chi)/\sin(\theta - \chi)$, χ being the cutting angle (all angles have signs, trigonometric convention). For symmetric reflection one has $\chi = 0$ and $b = 1$.

Let us apply the relation (1) to the monochromator–analyzer pair, not necessarily identical. One has to consider the situation after reflection on the monochromator and before reflection on the analyzer:

$$\Delta k/k = \cot\theta_M(b_M\xi_M - \gamma) = \cot\theta_A(\xi_A + \gamma). \qquad (2)$$

As the reflectivity variables ξ_M, ξ_A are much smaller than the variable of the angular divergence γ, relation (2) is practically satisfied for any γ when $\theta_A = -\theta_M$. The matching thus happens for flat crystals when the d-spacings are equal and the setting is parallel (+, −). The dispersion parameter $a_A = -\tan\theta_A/\tan\theta_M$ then equals 1.

Consider now the situation when the analyzer is rotated by an angle ϵ (the rocking angle) from the central position. Assume also that a scatterer is placed between the two crystals, changing the direction of neutrons by a small angle $2\theta_S$. Denoting the distances monochromator-to-analyzer by L_{MA} and sample-to-analyzer by L_{SA}, one has from geometry:

$$\gamma L_{MA} + 2\theta_S L_{SA} = y_A - y_M, \qquad (3)$$

where y_A and y_M are the spatial coordinates across the beam at the analyzer and monochromator positions. Relation (2) in the situation considered becomes:

$$\begin{aligned}\Delta k/k &= \cot\theta_M(b_M\xi_M - \gamma)\\ &= \cot\theta_A(\xi_A + \gamma + 2\theta_S - \epsilon).\end{aligned} \qquad (4)$$

From (3) and (4) one obtains:

$$\begin{aligned}\epsilon = {} & 2\theta_S[1 - (1 - a_A)L_{SA}/L_{MA}]\\ & + (1 - a_A)(y_A - y_M)/L_{MA} + a_A b_M\xi_M + \xi_A.\end{aligned} \qquad (5)$$

By averaging (5) over the distributions of the variables y_M, ξ_M, y_A and ξ_A (with zero mean values) one obtains the relation between the nominal rocking angle and the nominal scattering vector $Q \approx 2k\theta_S$ assigned to it [10]:

$$Q = k\epsilon/[1 - (1 - a_A)L_{SA}/L_{MA}]. \qquad (6)$$

For $a_A = 1$ one has the known result $Q = k\epsilon$ regardless of the sample position. However, for $a_A \neq 1$, that is for crystals in (+, +) setting or of different d-spacings, the Q-scale will depend on the sample position.

The Q-resolution width, ΔQ, is related to the rocking curve width $\Delta\epsilon$ (full width at half maximum, FWHM) through the same relation (6). In the Gaussian approximation one has $\Delta\epsilon = (8\ln 2\langle\epsilon^2\rangle)^{1/2}$, the

variance $\langle\epsilon^2\rangle$ being computed from (5) to be, for the situation of interest $a_A = 1$,

$$\langle\epsilon^2\rangle = b_{M^2}\langle\xi_{M^2}\rangle + \langle\xi_{A^2}\rangle, \tag{7}$$

meaning simply that the rocking curve is the convolution of the reflectivity curves of the two crystals. The contribution to $\langle\epsilon^2\rangle$ coming from the beam width was canceled by the $(1 - a_A)$ factor in the corresponding term in (5). The whole point of the two-crystal method is that the SANS resolution may not be affected by the angular divergence or the spatial width of the neutron beam (which are large), as it is defined by the rocking curve width (which may be narrow).

The phase space matching conditions for successive reflections on bent crystals have been discussed before [5, 15, 16] and their derivation will not be detailed here. The starting point is an extension of relation (1) to bent crystals. In that extension the spatial coordinate y becomes relevant, because the Bragg angle depends on where neutrons strike the crystal. Then in the corresponding extension of relation (2) to bent crystals, two coefficients (of the variables γ and y) are required to coincide. There result two matching conditions, which for the case of the pair monochromator–analyzer have the expression:

$$f_M^* = (L_{MA}/2)/(1 - 1/a_A), \tag{8}$$
$$f_A = (L_{MA}/2)/(1 - a_A),$$

where f and f^* (with corresponding subscripts) are the first and second focal lengths of the bent crystal, given by:

$$f = (R/2)\sin(\theta + \chi)\mathrm{sgn}(\theta + \chi), \tag{9}$$
$$f^* = (R/2)\sin(\theta - \chi)\mathrm{sgn}(\theta + \chi),$$

where R is the radius of curvature in the diffraction plane (by convention positive if neutrons strike the concave side) and the factor $\mathrm{sgn}(\theta + \chi)$ formally allows angles to have signs. The relation $f = bf^*$ holds (b is the reflection asymmetry parameter), so in transmission geometry (Laue, $\chi > \theta$, thus $b < 0$) the two focal lengths have different signs. Flat crystals correspond to $1/f = 1/f^* = 0$ and are seen to be required indeed by (8) when $a_A = 1$.

Relation (7) remains valid for bent crystals, provided the phase space matching is achieved by fulfilling conditions (8). Then the contributions from the beam angular and spatial widths are canceled and it is only the reflectivity curves (broadened by bending) that are convoluted, so the rocking curve is narrow again. The formulae for the reflectivity widths of bent crystals have been given before [16, 17] and will not be discussed here. It suffices to mention that one can adjust the reflection asymmetry parameter and the thickness of both crystals to balance the bent crystal reflectivity widths in (7) and thus achieve the best resolution–intensity compromise.

When there is no phase space matching, the reflected beam after the analyzer is narrow, both in angle and in spatial extent. On rocking the analyzer the reflected beam sweeps across it, the rocking curve is broad and the intensity is low. When matching occurs, the whole volume of the analyzer enters into reflection at once, the rocking curve is narrow and the intensity is high. The width of the reflected beam increases dramatically, both in angle and in spatial extent—this is precisely the reason for the intensity being maximal at matching.

On passing to bent crystals relation (6) stays valid. With flat crystals the case $a_A \neq 1$ is of no interest, as the rocking curve is then broad and its peak intensity low because of the phase space mismatch. With bent crystals, the phase space windows can be made to coincide at any value of the dispersion parameter a_A by suitably choosing the two crystals curvatures. At a given rocking curve width, the Q-resolution will be better at $a_A > 1$ and worse at $a_A < 1$ than for the $a_A = 1$ case. Both the Q-scale and the Q-resolution will generally depend on the sample position. A peculiar situation occurs when the sample is right in the middle between monochromator and analyzer while $a_A = -1$, that is for identical crystals in antiparallel $(+,+)$ setting. Then the expression (6) for Q diverges: all the small-angle scattering is seen at $\epsilon = 0$ and no scattering is seen outside the rocking curve. This allows determining the total SANS cross-section on the rocking curve peak.

For the monochromator to have a positive second focal length f_M^* (giving beam convergence and thus allowing spatial focusing), it is seen from the first relation (8) that one must have $a_A > 1$, that is the monochromator must have a larger d-spacing than the analyzer. It is natural then to use the lowest-index Si (111) reflection for the monochromator and a higher-index reflection, like Si (220) or (311), for the analyzer. The choice will be dictated by the available space (the L_{MA} distance) and the required Q-resolution. The analyzer first focal distance will be negative, but by choosing the transmission geometry one can make its second focal distance positive, which actually matters for spatial focusing. With bent crystals, high peak reflectivities, close to 1 for strongly reflecting planes, can also be reached in the transmission geometry [16].

A consideration of the spatial focusing with the SANS pair of crystals in parallel setting shows that when the matching conditions are fulfilled, the beam from the monochromator will go into a focus that is always situated after the analyzer. The sample cannot

thus be placed at the focus. However, the spatial focusing may still be strong enough to make the intensity gain over flat perfect crystals more than proportional to the resolution broadening. With the two crystals in anti-parallel setting ($a_A < 0$) the focus is between the crystals, so the sample can be placed at the focus. However, the Q-resolution, at the same rocking curve width, is then worse than with $a_A > 0$. One cannot have simultaneously a very high flux through the sample and an improved resolution. The choice depends on the experiment, on whether intensity or resolution is more important, but it is nice to have such an option available.

If a bent pre-monochromator is used, its phase space emergence window has to match the acceptance window of the monochromator, which is already set by the choice of the analyzer. For a bent perfect pre-monochromator the corresponding conditions are analogous to (8), with the distance from pre-monochromator to monochromator L_{PM} instead of L_{MA} and with $a_M = -\tan\theta_M/\tan\theta_P$ instead of a_A:

$$f_P^* = (L_{PM}/2)/(1 - 1/a_M); \qquad (10)$$
$$f_M = (L_{PM}/2)/(1 - a_M).$$

As $f_M = b_M f_M^*$, a condition imposed on the experimental configuration results from (8) and (10):

$$L_{PM}/L_{MA} = b_M(1 - a_M)/(1 - 1/a_A). \qquad (11)$$

It can be satisfied at given distances by controlling the parameter b_M of the reflection asymmetry. For instance, with a Si (111) monochromator and a Si (220) analyzer in (+,−) setting at a wavelength of 1.5 Å one has $a_A = 1.72$, and with a bent Si (111) pre-monochromator in (+,+) setting one has $a_M = -1$. For the ratio of the two distances one obtains thus $L_{PM}/L_{MA} \approx 4.8 b_M$. Incidentally, standard silicon ⟨111⟩ wafers for electronic applications have offset angles in the right range, allowing the fulfilling of this condition for typical distances in existing three-axis spectrometers. For a mosaic crystal pre-monochromator, owing to the larger extent of its phase space window, the matching condition relaxes. The pre-monochromator optimal curvature may differ significantly from that given by relation (10) and must be computed numerically.

3. COMPUTATIONS AND EXPERIMENTAL VERIFICATION

Detailed computations were performed with a neutron optics program (DAX) described elsewhere [17] in a version (SA) adapted to the SANS problem. Intensitites up to 400 times higher than with flat perfect crystals were computed to be obtainable with identical bent Si (111) crystals in anti-parallel (+,+) setting. However, the corresponding resolution degradation appears to be too severe. Of greater practical interest is the parallel (+,−) setting with different reflections of bent silicon. Intensity gains by factors of several tens to more than one hundred can be obtained, depending on the difference in d-spacings and the distance between crystals.

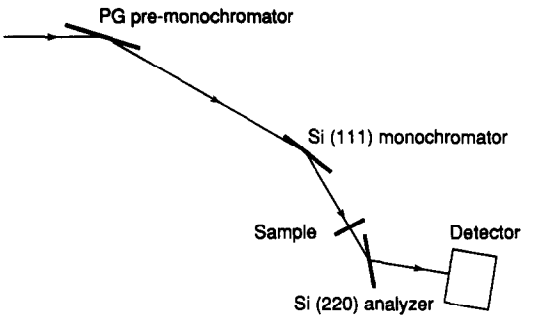

Fig. 1. Schematic view of the SANS bent-crystal arrangement implemented at MURR at a 1.5 Å neutron wavelength.

On the basis of these computations several arrangements were selected for possible use at ORNL, one of which has already been implemented there. An optimal arrangement for the MURR E-port three-axis spectrometer geometry was also computed and implemented. It consists (Fig. 1) of a bent pyrolytic graphite (PG) pre-monochromator, followed in (+,+) setting by a standard Si ⟨111⟩ wafer (0.64 mm thick) with (111) planes in asymmetric reflection, and then in (+,−) setting by a similar wafer with (220) planes in asymmetric transmission geometry. The distances $L_{PM} = 1.5$ m and $L_{MA} = 0.6$ m were dictated by the instrument geometry. To adapt to them, the monochromator had to use the inverse Fankuchen ($b_M < 1$) setting, with beam broadening. An offset angle of about 4° of standard ⟨111⟩ wafers allowed the condition (11) to be satisfied.

The pre-monochromator consisted of flat PG plates placed on a holder shaped cylindrically to the necessary radius (4.3 m). The thin monochromator wafer was spherically bent to 4.6 m in a vacuum device with the curvature set by controlling the sub-pressure with needle valves. The analyzer was mechanically bent to −5.8 m (convex) in a four-point device (to reduce the background from the crystal support). Some of the design computations and the corresponding experimental results are shown in Figs 2–6.

Figure 2 shows the intensity of the beam after the monochromator, as a function of the pre-monochromator curvature. The curvature of the Si (111) monochromator was set at the value ensuring the phase space matching with the Si (220) analyzer. The data in Fig. 2 are normalized to the beam intensity for a flat mosaic squashed-silicon (111) pre-monochromator which had been used in a

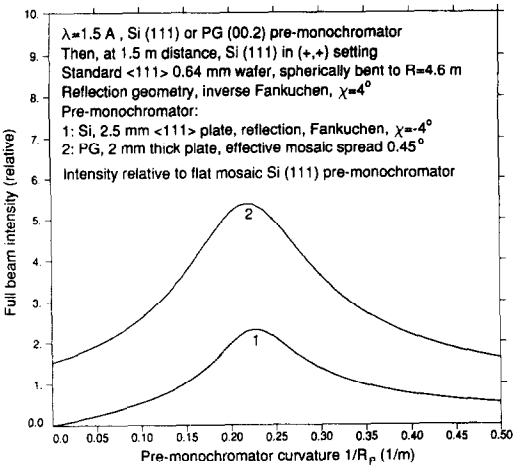

Fig. 2. Computed beam intensity after double reflection (by pre-monochromator and monochromator), as function of the curvature of the pre-monochromator. Curve 1 is for a perfect silicon (111) pre-monochromator in Fankuchen (beam condensation) setting. Curve 2 is for the PG pre-monochromator that was eventually implemented. Intensities are normalized to that for a flat mosaic Si (111) pre-monochromator.

preliminary SANS arrangement of the same type. Curve 1 is for a pre-monochromator consisting of a spherically bent perfect silicon plate, in a Fankuchen (beam condensation) setting. The corresponding intensity gain over the flat mosaic monochromator is limited by the need to set the plate thickness below the breaking limit. Curve 2 corresponds to the bent PG pre-monochromator that was eventually implemented. The gain in intensity by a factor of 5 was confirmed experimentally. However, the curve obtained by rocking the monochromator against the pre-monochromator showed some structure, due to the segmentation of the latter.

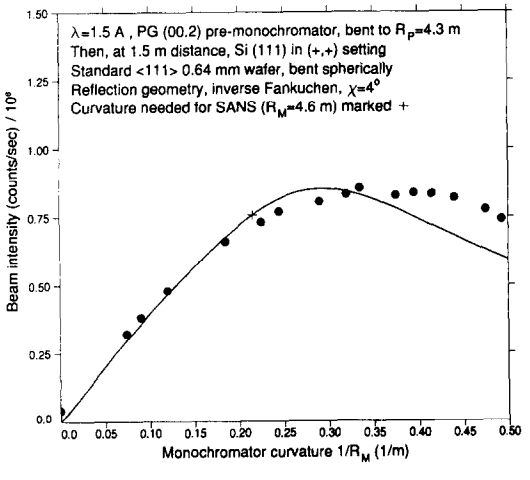

Fig. 3. Count rate after double reflection (by pre-monochromator and monochromator), as a function of the curvature of the monochromator (computation and measurement). The curvature of the pre-monochromator corresponds to the maximal intensity in Fig. 2.

Figure 3 shows in absolute units (count rate) the beam intensity after double reflection, by the pre-monochromator and then monochromator, as a function of the curvature of the monochromator. The theoretical curve, also computed in absolute units for a thermal flux of 10^{14} n/cm^{2}s, had to be scaled down by a factor of 0.7, which is essentially the transmission of a sapphire filter put in the white beam to reduce the fast neutron background. The slight discrepancy between computations and measurement at large curvatures is due, most probably, to the segmentation of the pre-monochromator.

Figure 4 shows the computed beam width as a function of the distance after the monochromator for two radii of curvature (4.6 m and 3.3 m). The first corresponds to the working curvature (marked in Fig. 3) with the beam converging to a weak focus situated after the analyzer position. The second puts the focus at the analyzer position, but then the matching of the monochromator with the analyzer no longer exists. The measurements showed agreement with the curves. Photographs of the neutron beam are shown for the two curvatures, at the sample position and at the analyzer position, respectively.

Figure 5 shows the width of the SANS rocking curve (analyzer rotated against monochromator), as a function of the monochromator curvature. The analyzer curvature had been set at the optimal value. A minimal rocking curve width of 0.048° was measured at the optimal monochromator curvature corresponding to the exact phase space matching.

The overall intensity gain factor, as compared with the previous configuration with a flat mosaic pre-monochromator (which was already a significant advance over flat crystal methods), was 3.5, that is less than the value of 5 observed after the monochromator. This is believed to be due again to the segmentation of the pre-monochromator. The rocking curve peak was about 250,000 counts/s for the full beam shown in Fig. 4. In the SANS measurements we usually reduced the beam size to accommodate smaller samples. Attenuators were needed for measuring the high count rates on the central part of the rocking curve, quite unusual for two-crystal SANS measurements.

Our three-axis instrument did not have enough precision in setting angles to allow the measurement of flat perfect crystal rocking curves and thus a direct determination of the corresponding intensity gain. The bent-crystal rocking curve width of 0.048° (173 seconds of arc) was broader by a factor of 130 than the theoretical rocking curve width for a flat perfect Si (111) pair in symmetric reflection (1.3 seconds of arc).

Figure 6 shows the width of the rocking curve as a function of the analyzer curvature (negative, with the

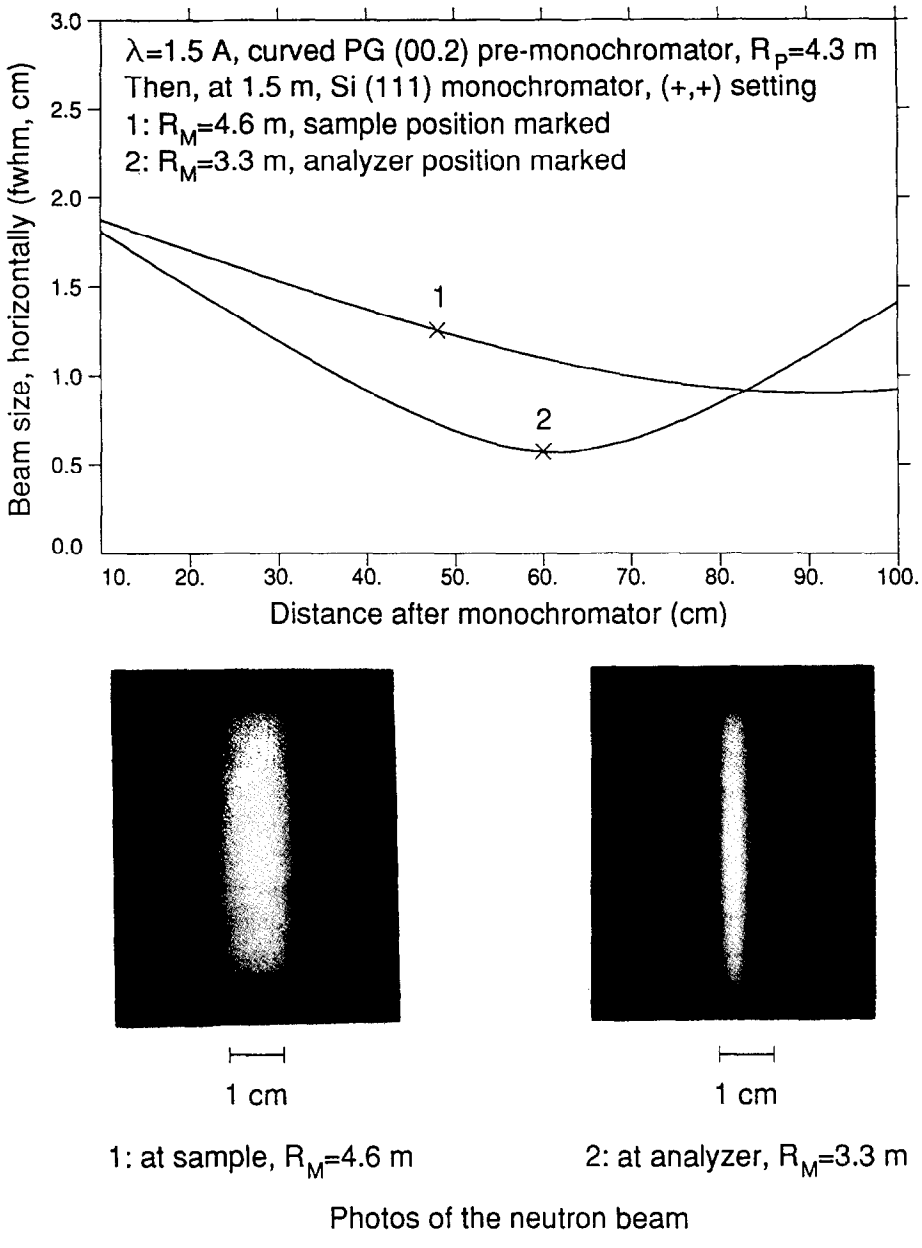

Fig. 4. Computed beam width as function of the distance after monochromator. 1: monochromator curvature set to the optimal value for SANS measurements. 2: monochromator curvature set to focus the beam at the analyzer position. Photos of the beam: at sample position for case 1, at analyzer position for case 2.

neutrons striking the convex side of the wafer in transmission geometry). Reasonable agreement is seen again between computations and observations. The curves in Figs 5 and 6 were measured in the working regime, with the incident beam limited to reduce the SANS background. With the full beam, the minima were more pronounced, but their positions and values at bottom were almost the same.

The Q-resolution corresponding to the 0.048° rocking curve width, computed through (6) for the sample placed at $L_{SA} = 0.12$ m, is 3×10^{-3} Å^{-1}. The measurements are illustrated in Fig. 7 with SANS data for a cement sample [14]. The rocking curve in the absence of sample is seen to drop quickly to the background level, which is about 10^{-4} of the peak intensity.

4. CONCLUSIONS

We believe that two important features of the bent-crystal SANS technique described here are versatility and high intensity. Arrangements with resolutions in a wide range, adapted to the physical problem to be investigated, can easily be implemented on existing three-axis spectrometers. Additional flexibility can

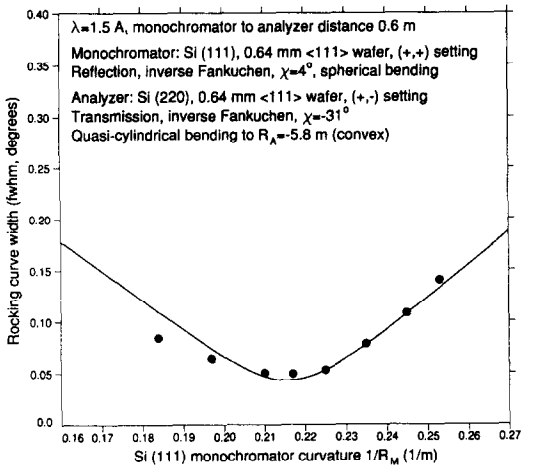

Fig. 5. Width of the rocking curve (analyzer against monochromator) as function of the curvature of the monochromator, with the analyzer curvature set at optimum. The phase space matching corresponds to the bottom of the curve.

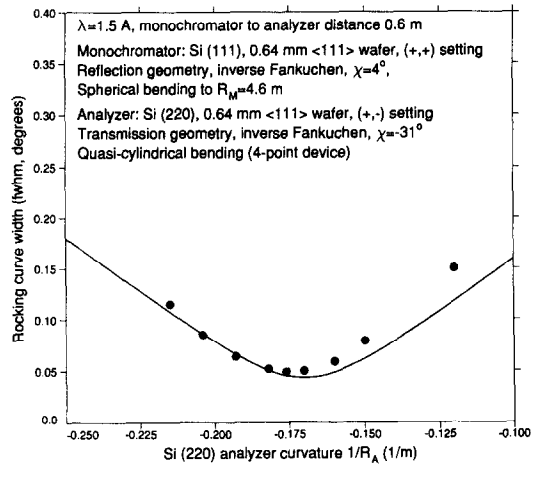

Fig. 6. Width of the rocking curve (analyzer against monochromator) as function of the curvature of the analyzer, with the monochromator curvature set at optimum.

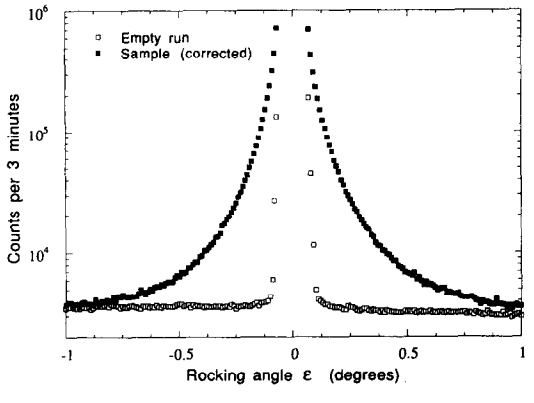

Fig. 7. SANS rocking curve data for the bent-crystal configuration: empty run and run with a 5 mm thick cement sample in the beam (corrected for sample transmission).

come from renouncing the constraints of fixed distances. With spatial focusing one achieves intensity gains larger than the resolution loss, in comparison with flat crystal arrangements. The fast data acquisition is especially useful for kinetic SANS studies [14, 15].

REFERENCES

1. Compton A. H. and Allison S. K., *X-Rays in Theory and Experiment*. Van Nostrand, New York (1935), repr. (1960); Fankuchen I. and Jellinek M. H., *Phys. Rev.* **67,** 201 (1945).
2. Schneider C. S. and Shull C. G., *Phys. Rev.* **B3,** 830 (1971).
3. Mook M. A., *J. Appl. Phys.* **45,** 43 (1974).
4. Bonse U. and Hart M., *Z. Phys.* **189,** 151 (1966).
5. Popovici M., Stoica A. D., Chalupa B. and Mikula P., *J. Appl. Crystallogr.* **21,** 258 (1988).
6. Popovici M. and Yelon W. B., *J. Appl. Crystallogr.* **25,** 920 (1992); *Nucl. Instr. Meth.* **A319,** 141 (1992).
7. Kulda J. and Mikula P., *J. Appl. Crystallogr.* **16,** 498 (1983).
8. Mikula P., Lukas P. and Eichhorn F., *J. Appl. Crystallogr.* **21,** 33 (1988).
9. Mikula P., Lukas P., Kulda J., Saroun J., Wagner V., Scherm R., Alefeld B. and Reinartz R., In *Neutron Optical Devices and Applications* (Edited by C. F. Majkrzak and J. L. Wood), SPIE Proc. Series, Vol. 1738, p. 411 (1992); Lukas P., Mikula P. and Strunz P., *Nucl. Instr. Meth.* **A338,** 111 (1994); Saroun J., Lukas P., Mikula P. and Alefeld B., *J. Appl. Crystallogr.* **27,** 80 (1994).
10. Popovici M., Yelon W. B., Berliner R. and Stoica A. D., *41st Annual Midwest Solid State Conference*, Columbia, MO, September (1993).
11. Popovici M. and Yelon W. B., *Neutron Optical Devices and Applications* (Edited by C. F. Majkrzak and J. L. Wood), SPIE Proc. Series 1738, p. 422 (1992); *Nucl. Instr. Meth.* **A338,** 132 (1994).
12. Popovici M. and Yelon W. B., *Z. Kristallogr.* **209,** 640 (1994).
13. Popovici M., Yelon W. B., Berliner R. and Heuser B. J., *MURR 1994 Annual Report*, pp. 95–96.
14. Berliner R., Heuser B. J. and Popovici M., *MURR 1994 Annual Report*, pp. 101–102.
15. Heuser B. J., Popovici M. and Berliner R., *MRS Fall Meeting*, Boston (1994).
16. Popovici M. and Yelon W. B., *J. Neutron Res.* **3,** 1 (1995).
17. Popovici M., Yelon W. B., Berliner R., Stoica A. D., Ionita I. and Law R., *Nucl. Instr. Meth.* **A338,** 99 (1994).